Chapter 7

Earth Observation for Urban Climate Monitoring: Surface Cover and Land Surface Temperature

Zina Mitraka and Nektarios Chrysoulakis

Additional information is available at the end of the chapter

http://dx.doi.org/10.5772/intechopen.71986

Abstract

The rate at which global climate change is happening is arguably the most pressing environmental challenge of the century, and it affects our cities. Climate change exerts added stress on urban areas through increased numbers of heat waves threatening people's well-being and, in many cases, human lives. Earth observation (EO) systems and the advances in remote sensing technology increase the opportunities for monitoring the thermal behavior of cities. The Sentinels constitute the first series of operational satellites for Copernicus, a program launched to provide data, information, services, and knowledge in support of Europe's goals regarding sustainable development and global governance of the environment. This chapter examines the exploitation of EO data for monitoring the urban climate, with particular focus on the urban surface cover and temperature. Two example applications are analyzed: the mapping of the urban surface and its characteristics, using EO data and the estimation of urban temperatures. Approaches, like the ones described in this chapter, can become operational once adapted to Sentinels, since their long-term operation plan guarantees the future supply of satellite observations. Thus, the described methods may support planning activities related to climate change mitigation and adaptation in cities, as well as routine urban planning activities.

Keywords: Earth observation, Copernicus Sentinels, urban climate, satellite remote sensing

1. Introduction

Global climate change is one of the most pressing environmental challenges of the century. Climate change is affecting cities and their residents, especially the poor ones, and more severe impacts are expected as climate extremes. Cities already face significant climatic and environmental challenges that are independent of climate change. They are generally warmer

than the surrounding non-urban areas, because of the higher heat absorption and the relatively limited cooling associated with vegetation and permeable surfaces. Urban areas suffer from air pollution, which is exacerbated by high temperatures. In conjunction with these existing issues, the impacts of climate change on cities will depend on the actual changes in climate, such as increased temperatures and rainfall.

The cities need to adapt and the climate change needs to be considered in all development plans and investments, local, national, and international. Local policy makers tend to see climate change as an environmental issue of global scale that is not of their concern. The majority of climate change specialists focus on reducing greenhouse emissions, without practically helping cities to learn how to change and adapt. Climate change science mainly deals with global and regional impacts, and it is less able to provide reliable assessments for the cities.

Datasets from Earth observation (EO) satellites are crucial for measuring key parameters relevant to the climate change. The use of satellites to observe the Earth provides the data necessary to improve our understanding of the Earth system and help predict future change. The satellite data and products may form the understanding of climate change and the quantitative estimates of its effects form the basis for policy-makers to build effective strategies for adapting to and mitigating the effects of a changing climate. Although EO data and products are mainly used for global and regional research studies, there is great potential in their use for monitoring the urban climate and thus allow cities to adapt to a changing climate.

1.1. The climate of cities and the urban scales

The urban climate refers to the specific climatic conditions in cities that differ from the surrounding areas, as an effect of the urban development. Urbanization tremendously changes the form of the natural landscape causing changes in the local climate, not only compared to the surrounding areas, but also inside the city. While some climatic elements differ only slightly from one city district to the other, like the precipitation for example, others differ significantly, like the temperature and the wind conditions.

In the case of conventional meteorological elements (temperature, humidity, wind, and precipitation), it is not as easy to establish the magnitude of modulation of the atmospheric boundary layer by a city, and it is even more challenging to assign causes for the observed changes. One of the main difficulties is the geographical setting of cities. The setting of a city is barely random and settlements are usually developed for specific reasons. Riverbeds, for example, offered good communications in earlier years; coastal cities were developed near natural harbors; others near to natural resources. In many developed countries, settlement sites were also selected because they were more readily defensible than others. In the majority of cases, the topography is rather complex and there were micro- and meso-climatic differences between the settlement sites and the surroundings even before the cities ever sprung up [1].

With the construction of buildings, parking lots, and houses, urban areas dramatically change the smoothness of a surface, the thermal conductivity, the hydraulic conductivity, the albedo,

http://dx.doi.org/10.5772/intechopen.71986

the emissivity, and the fraction of vegetation cover. Thus, urban regions behave a lot different from natural ones and they cause unique physical processes, depending on many parameters like the heat retaining capacity of the construction materials, the sealing of the soil, a modified water balance and the waste heat. As a result, urban landscapes modify the original physical processes that govern any natural land surface, and also add new, unique biogeophysical and biogeochemical processes into the land surface–atmosphere, such as the storage heat flux, the canyon effect, and the anthropogenic heat flux [2].

The urban surface and morphology results in cities being relatively warmer than the rural surroundings, a phenomenon called urban heat island (UHI). The warmer city climate can have fatal consequences such as those witnessed during the summer heatwave of 2003 in Central Europe [3]. There are different kinds of UHIs, displaying different characteristics and controlled by different assemblages of energy exchange processes. These possess different scale manifestations and result from different processes. Air temperature varies with height, a phenomenon much complicated in the urban environments and the different atmospheric layers. Thermal remote sensing permits definition of an UHI named ground or surface UHI, which refers to the skin or surface temperature difference between the city and its surrounding areas.

The concept of scale is fundamental in the understanding of the surface-atmosphere interactions when it comes to urban environments. In building scale, for example, the walls and roof facets have different time-varying exposure to solar radiation, net longwave radiation exchange, and ventilation. Horizontal ground-level surfaces are a patchwork of elements, such as irrigated gardens and lawns, non-irrigated greenspace, and paved areas with contrasting radiative, thermal, aerodynamic and moisture properties, frequently including trees. These different surface elements possess diverse energy budgets that generate contrasts in surface characteristics (e.g., skin temperature), and lead to mutual interactions by radiative exchange and small-scale advection. These fundamental units may be aggregated hierarchically, as illustrated in **Figure 1**.

Distinctive energy balances characterize each scale that generally do not represent the area-weighted average of the budgets of individual elements. This happens because each unit interacts with adjacent ones in the same scale by advection. While spatial scale increases, the

Figure 1. Graphical illustration of the different scales in the city. The urban canyon scale includes building walls and elements between buildings. The city block scale includes a number of urban canyons and roofs of buildings. The neighborhood scale refers to a number of city blocks, while the land use scale refers to larger areas including many similar neighborhoods.

spatial variability is likely to be reduced and less difference is expected among two land-use classes in a city for example, than between a north and south-facing wall of an individual building. Urban climatology studies this heterogeneity and complexity, either explicitly, in terms of detailed mapping of urban morphology, or in interpreting observations at aggregate scales [4].

1.2. Urban surface and morphology

The urban surface is composed of a large number of man-made materials arranged in a complex three-dimensional (3D) structure. Cities are built with artificial materials, such as cement, asphalt, brick, pebbles, or aggregates, which absorb and store radiation throughout the day and slowly release heat through the night. Moreover, streets, sidewalks, and parking lots are generally impervious, meaning that they do not allow the water to infiltrate into the soil. Since the urban environment is predominantly covered by artificial pavement, it is important to study the types of materials used and their individual characteristics. Impervious surfaces not only absorb high heat loads, which increase air temperatures through heat convection, but also increase the rate and temperature of runoff during storms [5].

While land changes from forests, grasslands, and croplands to impervious surfaces, the energy balance changes. The larger amount of solar radiation reaching the Earth's surface is reflected, absorbed, and transformed into sensible and latent heat. A small percentage of the solar radiation is also used in photosynthesis. The atmosphere close to the surface is mainly heated by energy radiating off the Earth's surface and not by direct solar heating. The surface materials affect largely the amount of solar radiation reflected or absorbed and, thus, they affect the heat flux from the surface to the atmosphere. The impervious surfaces alter the local energy balances through changes in the albedo, the emissivity, the specific heat capacities, and the thermal conductivities of the surfaces, as well as the ratio of sensible to latent heat fluxes from the surface to the atmosphere. Therefore, this impacts the temperature and humidity of the overlying air. Cool pavements are made from advanced materials and surface types that are used for decreasing the surface temperature in urban environments. These are mainly based on the use of materials with high albedo combined and high emissivity or techniques that exploit the latent heat to decrease the surface and ambient temperature [6]. Nevertheless, not only the materials, but also the 3D structures of the city have important impact on its radiational balance and thus its temperature. The shape of the cities can be described by several measures, each of which has effect on the city climate. The buildings and trees height affects the reflectivity, the flow regimes, and the heat dispersion above ground. The surface properties as well as the 3D structure of the cities can both be assessed using remote sensing methods and EO data.

2. Urban remote sensing and urban climate

A variety of remote sensors, satellite and airborne, detect and measure energy patterns from different portions of the electromagnetic spectrum, which are useful to quantify several

parameters essential for urban studies. The great number of EO data from satellite and airborne systems presents an opportunity to extract a great wealth of information via remote sensing, relevant to the urban and peri-urban environments at various spatial, temporal, and spectral scales. With recent innovations in sensor technologies, urban applications of remote sensing, i.e., urban remote sensing, has rapidly gained popularity among a wide variety of communities.

Environmental scientists are increasingly relying upon EO data to derive, for example, urban land cover information as a primary boundary condition used in many spatially distributed models [7]. The climate change community has also recognized remote sensing as an enabling and acceptable technology to study the spatiotemporal dynamics and consequences of urbanization as a major form of global changes [8]. Lately, more urban researchers are also using remote sensing to extract information for studying the urban surface and geometry [9, 10]. Finally, urban and regional planners are increasingly using EO data to derive information on cities in a timely, detailed, and cost-effective way to accommodate various planning and management activities [11].

Urban remote sensing can help improve our understanding of cities and many benefits of using EO data for urban studies that can be identified. The largest benefit of remote sensing, its capability of acquiring images that cover a large area, applies also for urban studies, where synoptic views allow identifying objects, patterns, and human-land interactions. Identifying the urban processes that operate over a rather large area and quantifying the differences in an intra-urban level is essential for understanding the urban environment. Remote sensing provides a great asset on information gathering on the entire mosaic of an urban phenomenon, while knowledge and expertise from multiple disciplines can lead to full understanding and modeling the urban processes.

Remote sensing holds an advantage as well, and complements the field measurements. Field measurements in most cases in urban sites do not represent the broader area. To cover large areas a lot of field measurements are needed, dense in both temporal and spatial terms and this can become prohibitively expensive in most cases. Moreover, data collected from field surveys and measurements can suffer from biases in the sampling design. Remote sensors can collect data in an unbiased and cost-effective way and thus provide better insights on the spatial and temporal evolution of processes. Field measurement can complement the remote sensing ones and combined methods and products hold great potential in terms of accuracy, spatial, and temporal coverage.

A framework of monitoring, synthesis, and modeling in the urban environment can be achieved with synergies of EO data integrated with relevant geospatial technologies, like spatial analysis and dynamic modeling. This framework can then be used to support the development of a spatio-temporal perspective of the urban processes and phenomena across scales and also to relate the different human and natural variables for understanding the direct and indirect drivers of urbanizations.

Last, remote sensing is ideal for connecting different scales for urban studies. Urban science disciplines have their own preferred scales of analysis. For example, urban planners tend to

work at street and neighborhood scales, while regional planners deal with larger entities such as metropolitan areas, even a whole city, or country region. Urban ecologists work at many spatial scales defined by the ecological units, and so as urban geographers, depending upon the specific topics under investigation. Urban meteorologists define the scales by the different physiographical features of the city. EO data can provide global coverage with spatial resolution ranging from sub-meter to a few kilometers and with varying temporal resolutions. The different urban researchers use different temporal scales depending on their application, varying from hourly, daily, weekly, monthly, seasonally to annual or decal basis. EO data allow work at any scale depending on the urban phenomenon being examined and they also offer the unique potential for linking different scales.

Remote sensing improves our understanding of urban areas in several ways, although the complexity of the urban environment challenges the realistic potential for making these improvements. Despite the profound benefits of using EO data for urban studies, the great inhomogeneity of urban environments obstructs the applicability and robustness of remote sensing methods. The presence of manmade materials and structures and the variety of vegetation cover, along with the 3D nature of cities, cause substantial inter-pixel and intra-pixel variations, complicating the characterization of urban landscapes. A great scientific challenge lies in the combination of EO data from different sensors, both in terms of scales and type of measurements. Moreover, it is always a challenge to integrate satellite data with other types of geospatial data in urban environmental analyses, like field measurement data, and cope with the fundamental differences in data sampling and measurement.

The ability to map, monitor, and analyze the complex and dynamic attributes of urban environments from EO data greatly depends on the characteristics of the remote sensing imaging instrument. Operational satellite EO systems are designed for specific missions, and thus have different operational principles and technical characteristics depending on the specifications of the missions. Currently, no EO system is specifically designed for monitoring urban areas. Airborne imaging systems are more flexible, but the cost of airborne campaigns limits the frequency of acquisitions and the area of coverage.

2.1. Satellite data in urban studies

A large variety of satellite data can be used for urban studies. The selection of a particular data source is a compromise among data availability, costs, and the required spatial, spectral, and temporal resolution. The majority of urban phenomena are scale-dependent, which means that urban patterns change with the scale of observation. Urban processes appear to be hierarchical in pattern and structure [12]. Therefore, studies of the relationship between the patterns at different levels in the hierarchy are urgently needed in obtaining a better understanding of the scale and resolution requirements in urban areas and in finding the optimal scale for examining the relationship between urban landscape pattern and process.

Over the past decade, urban remote sensing has emerged as a new frontier in the EO technology by focusing primarily on mapping and monitoring of the urban land cover and its spatial extent. The line in **Figure 2** shows the number of journal articles (including review articles)

http://dx.doi.org/10.5772/intechopen.71986

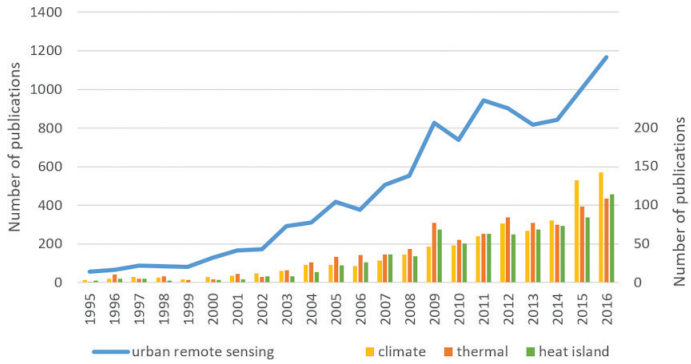

Figure 2. The number of journal articles (including review articles) including the key words urban remote sensing (line), urban remote sensing climate (first set of bars), urban remote sensing thermal (second set of bars), urban remote sensing heat island (third set of bars). Source: Scopus search on August 18, 2017.

on urban remote sensing, since 1995. There is a published literature on urban remote sensing since the 1970s, but a highly increasing rate is observed around 2002. This period coincides with the advent of very high spatial resolution satellite images (higher than 5 m) and the first spaceborne hyperspectral images. Thus, enhanced image processing techniques were developed such as the object-based image analysis, data mining, and data and image fusion of different sensors, wavelength regions and spatial, spectral, and temporal resolutions.

The same trend can be noticed in the literature of urban remote sensing for climate (first set of bars in **Figure 2**), which has been following similar rate of increase in these years. It is interesting though to observe that the pattern of urban thermal remote sensing (second set of bars in **Figure 2**) follows very close the one of urban heat island (third set of bars in **Figure 2**). Although expected, this graph is a strong indication that, so far, when referred to urban climate monitoring from space, the main focus is usually in thermal remote sensing. It is indeed true that thermal remote sensors provide indispensable information for the surface temperature, with their great advantage being the spatial cover of large areas. Yet, remote sensing can contribute much more than that into our understanding of the biophysical properties, the patterns and the processes of urban landscapes using all ranges of electromagnetic wavelength and active sensors as well. In fact, the last year (2015–2016) seems that the remote sensing community has started publishing studies related to urban climate, which are not necessarily using thermal data or are referring to the urban heat island.

From the wealth of available and upcoming EO data, detailed information on the urban surface cover and quantitative estimates of the biophysical parameters related to the urban climate can be extracted. Methodologies that exploit and combine satellite data from different sources and of various spatial, spectral, and temporal resolutions can give insights on the evolution in space and time of the urban climatic phenomena. Current and upcoming satellite sensors may provide great wealth of information for our understanding of the cities climate. Remote sensing provides a wealth of data of different spatial, spectral, and temporal resolutions that can cope with the spatial and temporal scale requirements of urban climate studies.

2.2. Spatial, spectral, and temporal resolutions for urban climate studies

Although the operating principles of various imaging instruments have changed over the years, the spectrum of applications and usability of imagery have been largely determined by their spatial, spectral, and temporal resolutions. Image resolution characteristics play a major role in determining the size and properties of the features or phenomena that can be discriminated in remotely sensed imagery.

The spectral signal is one of the most important properties of urban land surfaces measured with remote sensing. Most satellite sensors are multispectral systems, meaning they sense the earth surface with a few broad spectral bands. Urban environments possess a high spectral heterogeneity and they are characterized by a large diversity of materials. Therefore, increased spectral resolution is a requirement for urban remote sensing.

The spatial resolution of remote sensor is a function of the altitude of the platform relative to the earth surface and the resolving power of the sensor. The spatial resolution is often expressed as the ground sampling distance of the sensor at nadir. The spatial resolution required for a given study could be determined by the size of the smallest element to be mapped. However, due to several factors, the element spatial resolution is not sufficient to detect urban objects. The radiation measured for one pixel is affected by the radiation of its neighboring pixels, due to scattering effects that complicate the analysis. Moreover, an object can only be positively identified if it is represented by several pixels. The ideal spatial resolution of an image for a given application will, therefore, be several times smaller than the size of the smallest object that needs to be identified.

The Nyquist sampling theorem [13] establishes a sufficient condition for a sample rate that permits a discrete sequence of samples to capture all the information from a continuous-time signal of finite bandwidth and it is the theoretical basis for the spatial resolution needed to map individual objects. The Nyquist theorem suggests that an object should be of the order of one-tenth of the dimension of the pixel in order to ensure that it will be completely independent of its random position and orientation relative to the sampling scheme. A schematic representation of the relationship between the spatial resolution and the objects under consideration is given in **Figure 3**, although applicable thresholds are not easy to define. The three situations outlined in **Figure 3** require different approaches to unravel information for the underling objects. The urban surface objects (i.e., buildings, roads, etc.) have small spatial extent. Given the large amount of spatial heterogeneity, most analyses in urban areas rely upon high spatial resolution imagery usually from aerial photography or drones.

EO data and the advances in remote sensing techniques, though, can provide an alternative when working with larger scales than the objects to identify. The so-called sub-pixel classification methods resolve the radiance of a single pixel and identify percentages of separate components. These methods are particularly useful for material mappings when used with hyperspectral data [14], but there are examples in the literature of sub-pixel classification methods used with coarser spectral and spatial resolution data [15, 16].

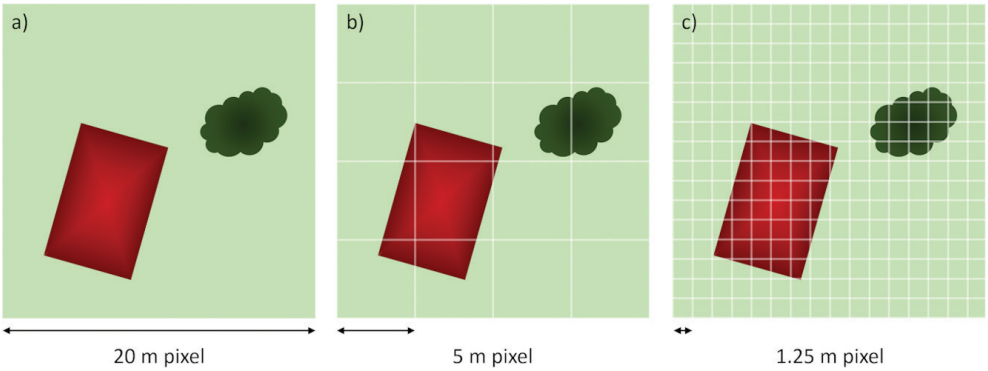

Figure 3. Relationship between objects under consideration and spatial resolution in urban sites: (a) pixels significantly larger than objects, (b) pixel and objects sizes are of the same order, and (c) pixels are significantly smaller than object.

The temporal resolution of a remote sensing system is the theoretical or the operational capability for acquiring repetitive imagery over some time interval. The spatial extent of images depends on the swath width, and influences the resulting temporal resolution.

A wide variety of EO systems acquiring data with various resolutions can be useful for urban studies. Medium resolution remote sensor data have been used to examine large dimensional urban phenomena or processes since early 1970s when NASA successfully launched the first Landsat. Over a period of nearly four decades, the Landsat program has acquired a scientifically valuable image archive unmatched in quality, details, coverage, and length, which has been the primary source of data for urbanization studies at the regional, national, and global scales. Since July 1982, with the launch of Landsat 4, thermal sensors are included in Landsat missions enabling surface temperature studies. The Advanced Spaceborne Thermal Emission and Reflection Radiometer (ASTER), a cooperative effort between NASA and Japan's Ministry of Economy Trade and Industry (METI), in orbit since December 18, 1999, includes a multispectral thermal instrument, which provides accurate estimates of emissivity and surface temperature in high spatial resolution. Yet, its on-demand acquisition mode limits the spatial resolution.

2.3. The Sentinels

The Sentinels constitute the first series of the ESA operational satellites for the Copernicus Programme. Copernicus is the continuity of the Global Monitoring for Environment and Security (GMES) Programme, which is launched to provide data, information, services, and knowledge that support Europe's goals regarding sustainable development and global governance of the environment. Copernicus is a European system for monitoring the Earth. It consists of a complex set of systems, which collect data from multiple sources: EO satellites and *in-situ* sensors and provides up-to-date information through a set of services related to environmental and security issues. The five Sentinel missions are based on constellations of two satellites to fulfill revisit and coverage requirements, providing robust datasets for Copernicus.

The Sentinel-2 mission provides continuity to services relying on multispectral high-spatial-resolution optical observations (like Landsat and SPOT satellites): it carries a Multispectral Instrument (MSI) covering the electromagnetic spectrum from the visible to the shortwave infrared with a pixel resolution from 10 to 60 m. Two satellites in orbit will provide data at a 5 days interval at the equator. Sentinel-2 combines a large swath, frequent revisit, and systematic acquisition of all land surfaces at high-spatial resolution and with a large number of spectral bands [17]. The pair of Sentinel-2 satellites routinely delivers high-resolution optical images globally, providing enhanced continuity of SPOT and Landsat type data.

Sentinel-3 mission represents the continuity of the ENVISAT sensors, i.e., MERIS (MEdium Resolution Imaging Spectrometer) and Advanced Along Track Scanning Radiometer (AATSR). In particular, the Sea and Land Surface Temperature Radiometer (SLSTR) will provide TIR data at 1 km resolution with daily revisit at the equator [18]. Among the Sentinel-3 mission objectives is to monitor the land surface temperature with high-end accuracy and reliability in support of climate monitoring.

3. Application for surface cover and land surface temperature

This chapter examines the exploitation of EO data for monitoring the urban climate, with particular focus on satellite data. The mapping of the urban surface and its characteristics, using spectral unmixing is examined in the first part. A method adjusted for urban studies is proposed which accounts for the non-linear mixture of spectral radiances in the urban canyon. The second part focuses on thermal EO data. To capture the intra-urban variations of temperature, EO data of high spatial and temporal resolution are necessary, but no current of forthcoming satellite provides them. Moreover, only one from the series of Sentinel satellites carries a thermal sensor of low spatial resolution. To overcome the limitations of the resolution trade-off, a synergistic methodology between high resolution optical and low resolution thermal satellite measurements with ultimate goal daily local-scale land surface temperature estimates.

3.1. Test area and data

The test area is in the city of Heraklion, Greece, and it covers an area of about 90 km^2. It is a typical Mediterranean city, characterized by mixed land-use patterns that include residential, commercial and industrial areas, transportation networks and rural areas. **Figure 4** shows the Urban Atlas land use map of Heraklion [19]. Apart from the Heraklion city core, the rest of the study area is featuring mixed urban and agricultural land cover pattern, mainly olive trees and vineyards.

Fourteen cloud-free Landsat 8 Surface Reflectance Climate Data Record (CDR) covering the test area corresponding to 1 year (April 1, 2013–April 30, 2014) were used in this study. The Landsat 8 CDR is a higher level data product of surface reflectance information for six bands,

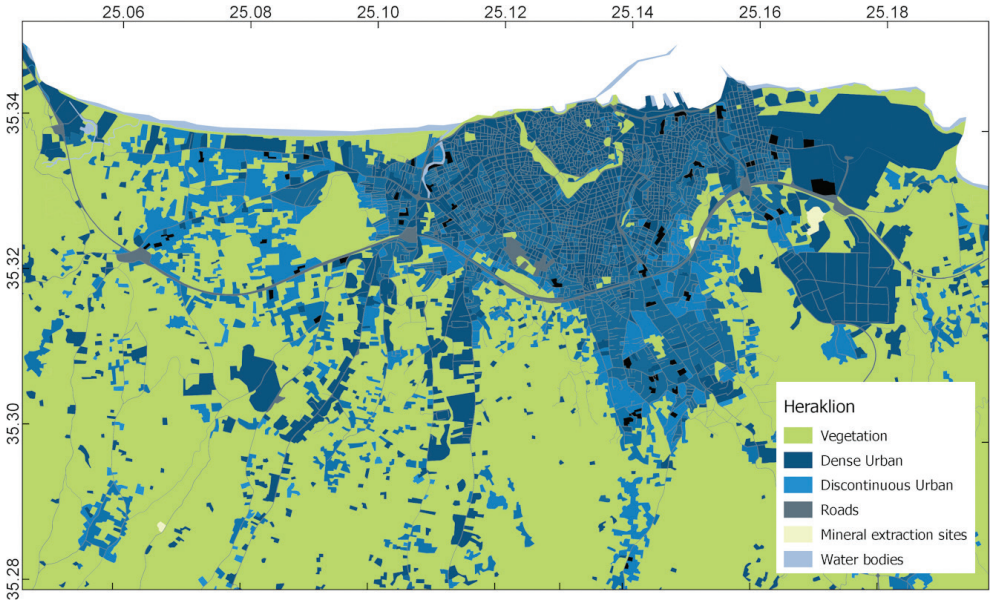

Figure 4. Urban Atlas land use polygons of the test site, the city of Heraklion, Greece.

generated from Landsat Ecosystem Disturbance Adaptive Processing System (LEDAPS) distributed by the U.S. Geological Survey [20].

Daily MODIS Level 1B (MOD021) data from both Terra and Aqua satellites for a period between April 1, 2013 and April 30, 2013 were acquired. The daily MODIS water vapor product (MOD05) was also used to provide ancillary atmospheric information on water vapor and cloud cover.

3.2. Urban surface cover mapping

The sub-pixel land cover information was estimated using spectral unmixing with a neural network, trained using endmember spectra collected from the image and synthetic spectra [21]. The methodology applied to produce the synthetic spectra and to estimate the surface cover fractions is briefly described below.

The urban surface is assumed to be composed of four land cover types: built-up surface, vegetation, non-urban bare surfaces, and water bodies. Using Landsat imagery, it is not easy to discriminate between different materials, but rather surface cover types, due to the medium spatial and low spectral resolution [22]. Thus, a redundant two-level hierarchy is assumed, as shown in **Figure 5**, including the four main surface cover types in the first level and a more detailed one in the second level, serving the endmembers collection.

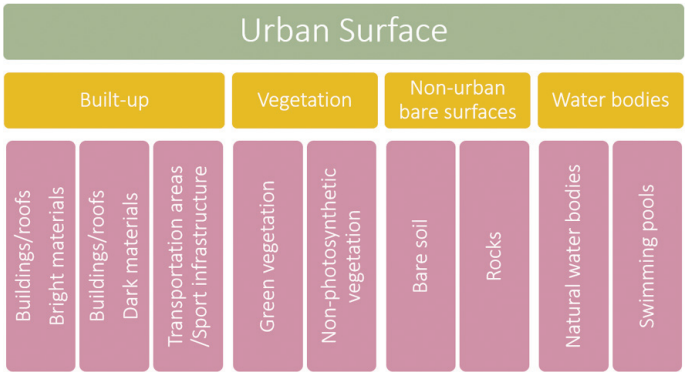

Figure 5. The two-level hierarchical urban classification scheme used in this study.

Endmembers are collected from the image corresponding to the second level of the hierarchy. This ensures a variety of different endmember spectra in the library, representing different surface cover types, rather than a single category. It has to be noted here that the endmembers collected from medium resolution imagery do not correspond to material spectra, but rather spectra of large homogeneous surfaces. The spectral resolution of Landsat (30 m) is not enough to discriminate between types of the second level of hierarchy. The collected endmembers are then grouped to match the surface cover types of the first level.

The median value of each Landsat pixel surface reflectance for the total six images was estimated. The reason for doing this was to create a single image corresponding to the whole year and to avoid extreme reflectance values. The thermal and panchromatic bands were not included in the analysis. The median reflectance product is an image covering 1 year (April 1, 2013–April 30, 2014). This image is used for the collection of the endmember. The median is selected as a statistic to avoid extreme values, which might cause confusions in the network training and the unmixing process. A number of endmember spectra, corresponding to the cover types of **Figure 5**, is collected from the median reflectance product by visual inspection and using high resolution imagery from Google Earth as reference.

The endmember spectra are then used to produce synthetically mixed training data. These are generated using models corresponding to the first level of the classification scheme (**Figure 5**). Two- and three-endmemeber mixture models are considered, with repeated surface cover types allowed inside a model. **Table 1** shows the models that are considered for the spectral unmixing. No water endmembers are considered in the models and the generation of synthetic spectra, because water is generally dark and highly degenerate in terms of spectral mixture [15]. Both linear and non-linear mixture models are then considered for the generation of synthetic spectra.

The linear mixing model assumed is described by:

$$\rho_i = \sum_{j=1}^{M} a_j(i) \cdot \rho_j, \forall a_j(i) \geq 0 \; and \sum_{j=1}^{M} a_j = 1 \tag{1}$$

Three endmember	Two endmember
BU + VE + NB	BU + BU
BU + BU + VE	BU + VE
BU + BU + NB	BU + NB
BU + BU + BU	VE + NB

BU, Built-up; VE, Vegetation; NB, Non-urban bare.

Table 1. Mixture models assumed for spectral synthesis.

where ρ_i is the observed spectrum of pixel i, ρ_j is the representative spectrum of endmember j, and M is the number of endmembers in the mixture model. The abundance coefficients $a_j(i)$ represent the areal fraction of the endmembers ρ_j in the pixel i. The linear model assumes that the surface corresponding to a pixel is flat and uniformly irradiated. This simple model representing the spectrum ρ_i as a linear combination of the endmember spectra ρ_j is rather popular [23]. Using the endmember spectra for each cover type, for all the models in **Table 1** and assuming combinations of different mixture levels $a_j(i)$, mixed spectra ρ_i are produced.

Although many studies assume linear mixing effects, it has been known for some time that non-linear spectral mixing effects can be a crucial component in many real-world scenarios, including the urban scenes [24]. The buildings and the street canyons create a complicated 3D structure in the cities at a meter scale, which induces multiple scattering of light between surfaces. Recently, a physics-based approach of a spectral mixture model suitable for urban scenes was presented and validated against simulated urban scenes using a quadratic mixing model [25]:

$$\rho_i = \sum_{j=1}^{M} a_j(i) \cdot \rho_j + \sum_{j=1}^{M} \sum_{l=j}^{M} b_{j,l}(i) \cdot \rho_j \rho_l \tag{2}$$

where the $\sum_{j=1}^{M} a_j(i) \cdot \rho_j$ accounts for the linear mixing, while $\sum_{j=1}^{M} \sum_{l=j}^{M} b_{j,l}(i) \cdot \rho_j \rho_l$ accounts for the non-linear interactions in the urban structure. The abundance coefficients $a_j(i)$ represent the areal fraction of the endmember ρ_j in the pixel i and the endmember spectra are used, for all the models in **Table 1**, with randomly generated $b_{j,l}(i)$ coefficients to produce synthetic spectra.

A three-layer feed-forward neural network with a sigmoid activation function was used in this study. The input layer has six neurons, one for each Landsat band and four output neurons, one for each of the land cover types of the first level (**Figure 5**) and a hidden layer with 12 neurons. The number of hidden neurons is set to 12, because the network performance would not improve much by adding more neurons. The network is trained using a Levenberg-Marquardt backpropagation algorithm and endmember and synthetic spectra from the developed spectral library. The network training data output is set to a combination of values in the interval [0,1], matching the coefficients $a_j(i)$ used during the spectral synthesis. Once trained, the network is then applied to estimate the surface cover fractions individually for the Landsat scenes.

The developed spectral library contains 15 endmember spectra, 2 representing buildings/roofs bright materials, 2 representing buildings/roofs dark materials, 3 transportation areas (roads, parking lots, and airport runways), 1 sport infrastructure, 3 green vegetation, 1 non-photosynthetic vegetation, 2 bare soil, and 1 rocks. Synthetic spectra were generated from these endmembers using the two- and three-endmember models presented in **Table 1**. In the end, a set of 72,030 synthetic spectra were used to train the neural network. Randomly chosen 70% of the spectral library data were used for training, 15% for validation and 15% for testing the neural network. The topology of the network was determined to be 6-12-3 input-hidden-output neurons and the Levenberg-Marquardt backpropagation algorithm was used to estimate the weights and bias values of the network. Derived estimates were then applied independently in the series of 14 Landsat images, and cover fraction images for the four land cover types assumed in this study were generated.

An example of the resulting surface cover fraction maps for May and August is shown in **Figure 6**. The general pattern shown in **Figure 6** matches the Urban Atlas polygons (**Figure 4**). Moreover, the fraction image corresponding to May reveals more vegetation abundance than the one corresponding to August both in the outskirts as well as in the urban core.

3.3. Urban land surface temperature

Although LST is routinely derived by satellite TIR observations, currently there is no space-borne sensor capable of providing frequent thermal imagery at spatial resolution needed in urban studies. Current and forthcoming TIR remote sensing is confronting the trade-off between spatial and temporal resolution. A synergistic method that unmixes the low-resolution TIR measurements using high spatial information on the surface cover for estimating high spatial resolution LST is applied here [26]. The method is a multistep procedure described in detail along with its validation in Ref. [26]. For the method to be applied, information on the surface cover fractions is necessary. Representative emissivity values are then assigned to each of the cover types in **Figure 5**, using information derived from the ASTER Spectral Library [27]. Samples from the library, which are representative for the study area, are selected and convolved with the sensor's spectral response function and the emissivity $\varepsilon_k^{(H)}$ for each pixel high resolution (H) pixel i is estimated by:

$$\varepsilon_k^{(H)} = \sum_{i=1}^{n} \varepsilon_i \cdot a_{ik}^{(H)} \tag{3}$$

where n is the number of surface cover types, ε_i is the representative emissivity value for the surface cover type i, and $a_{ik}^{(H)}$ are the estimated fractions of surface cover types.

Spatial-spectral unmixing is then used to enhance the spatial resolution of the low resolution thermal bands. The contribution of the land cover components is estimated for each thermal pixel k, by summing the estimated fractions $a_{j_i}^{(H)}$:

$$A_{k_i}^{(L)} = \frac{1}{P} \sum_{j \in P} a_{j_i}^{(H)} \tag{4}$$

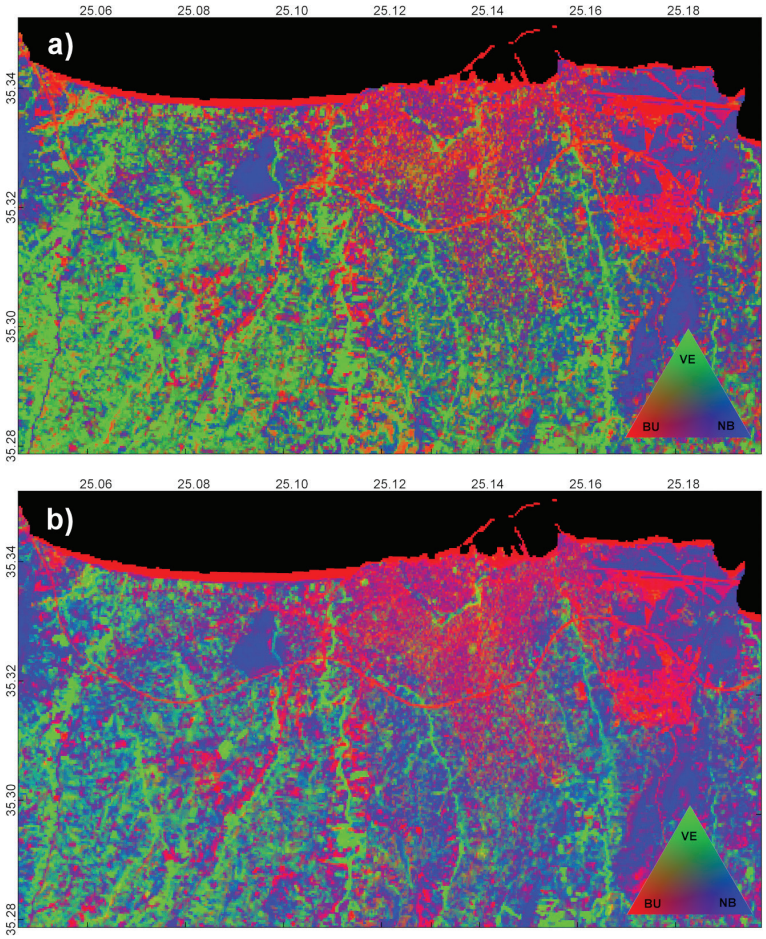

Figure 6. Pseudo color composition of the derived fraction images for the May 13, 2013 (a) and August 22, 2013 (b).

where P is the number of high resolution pixels ($j \in P$) corresponding to each low resolution one (k). Each low resolution pixel is then unmixed, using the contextual information of the neighboring pixels in a window (a window of size w):

$$\underset{w\times 1}{\underline{S}^{(L)}} = \underset{w\times n}{\underline{A}^{(L)}} \cdot \underset{n\times 1}{\underline{E}} + er \tag{5}$$

where $S^{(L)}$ is a vector of the thermal radiances of the pixels in the window, $A^{(L)}$ is a matrix of the contributions of surface types to those pixels, and E is the thermal radiances under consideration. A regularization term is also used to prevent large deviations in optimization:

$$min_E \left\| \boldsymbol{S}^{(L)} - \boldsymbol{A}^{(L)} \cdot \boldsymbol{E} + b \frac{w^2}{n} (\boldsymbol{E} - \boldsymbol{S}'^{(L)}) \right\|_2^2 \quad (6)$$

where $\overline{S'^{(L)}}$ are predefined spectra corresponding to surface cover types and b is a regularization parameter to ensure small spectral variations. The high spatial resolution thermal band is then constructed by applying Eq. (5) for high resolution (H).

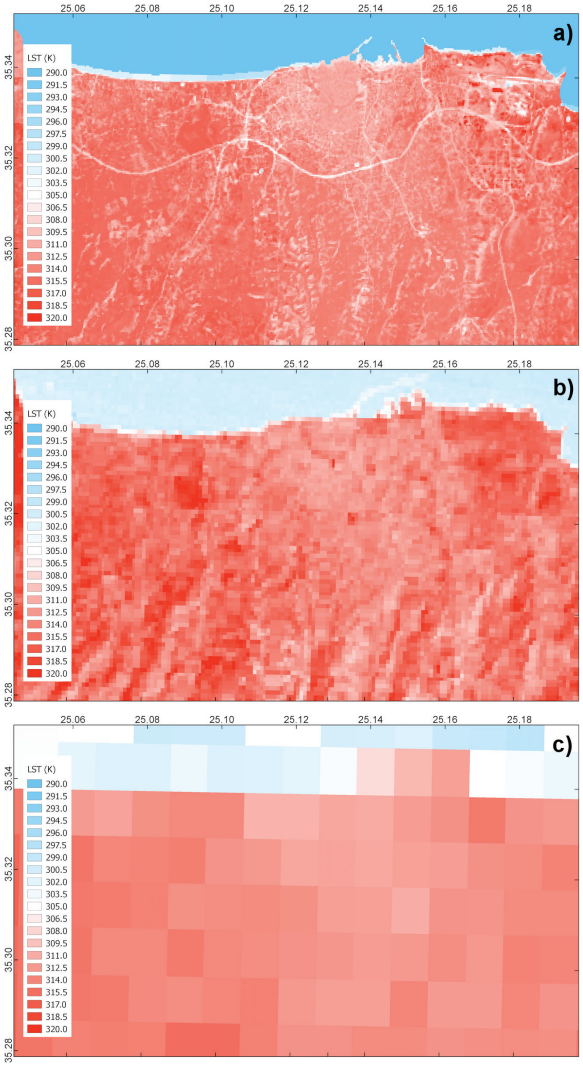

Figure 7. An example of downscaled LST (K) for the August 30, 2013 (a). The ASTER (b) and MODIS (c) LST products corresponding to the same date are also presented for comparison.

Given high resolution brightness temperature products for two thermal bands (T_i, T_j) and the respective emissivity products (ε_i, ε_j), LST is derived in high spatial resolution using a split-window algorithm [28]:

$$LST = T_i + c_0 + c_1 \Delta T + c_2 \Delta T^2 + (c_3 + c_4 WV)(1 - \varepsilon) + (c_5 + c_6 WV)\Delta\varepsilon \quad (7)$$

where WV is the atmospheric water vapor content, $\varepsilon = (\varepsilon_i + \varepsilon_j)/2$, $\Delta\varepsilon = \varepsilon_i - \varepsilon_j$, and c_0-c_6 are the split-window coefficients determined from the algorithm calibration.

The LST downscaling method was applied to the series of daily MODIS and a time series of daily high resolution LST (90 m) was derived for the case study. **Figure 7** shows an example of the methodology application for a cloud-free day (30 August, 2013) for which the ASTER LST product was also available. **Figure 7a** shows the high resolution LST, derived using the above-described downscaling procedure. The ASTER (**Figure 7b**) and MODIS (**Figure 7c**) LST products corresponding to the same date are also presented for comparison. The general temperature pattern of the downscaled LST product is similar to the ASTER LST product. The level of detail that appears in the downscaled product (**Figure 7a**) compared to the ASTER LST product (**Figure 7b**) is because the downscaled product is of 30 m spatial resolution (matching the Landsat-derived surface cover fractions), while the ASTER LST product is of 90 m spatial resolution.

4. Discussion

Medium spatial resolution satellite data have been used in the past with spectral unmixing methods for mapping the urban surface cover [15]. This chapter demonstrated the use of image endmember and synthetic spectra to estimate sub-pixel information on the urban surface cover. The proposed methodology is fast in terms of computational time and affordable to implement and apply for urban studies. It is also easy to reproduce for other cities, if the relevant data are available. It is, thus, suitable for monitoring the surface cover and it can be used for change detection and time series analysis. The products are useful for various studies, related to surface cover properties, urban climate, urban climatology, and urban expansion.

An example use of this detailed urban surface cover information is the LST downscaling method. The method described and applied in this chapter is highly dependent on accurate surface cover information. It has been demonstrated than the uncertainty in the downscaled LST estimation is closely linked to the uncertainty related to the surface cover fractions [29]. The methodology for mapping the urban surface cover is applicable to Sentinel-2 imagery. The enhanced spatial and spectral resolution of Sentinel-2 compared to Landsat is expected to advance the method. The optical bands of Sentinel-2 are similar to the ones of Landsat 8, but the enhanced spatial resolution of 10 m provides better insights on the underlying objects. Further advances may include analysis of the 10 m bands for identifying pure spectra to be used as endmembers for spectral unmixing techniques. Moreover, the additional bands

in the near-infrared compared to Landsat, for example, provide more spectral information necessary for unmixing techniques. Although these bands are designed for detecting and discriminating between different vegetation types, and their main advantage lies in this kind of applications, they can be proven useful for differentiating between urban materials as well. Further analysis is, though, needed to come to conclusions on using the red-edge bands for urban monitoring. Finally, Sentinel-2A and Sentinel-2B will provide frequent acquisitions with a revisit of 5 days in the equator and, in combination with the large swath of 290 km, the potential of updating the surface cover information is significantly increased. Thus, the increased temporal resolution substantiates the urban surface cover monitoring even in areas with persistent cloud cover.

The application of the downscaling method described in this chapter was demonstrated through an example using MODIS thermal data. With the use of the Sentinel-2 imagery, the surface cover characterization is expected to be improved significantly as discussed earlier. Moreover, the OLCI spectral bands measuring in VNIR share some common bands with Sentinel-2 MSI and this may allow further exploitation for updating the surface cover. Since, the Sentinels are developed for synergies [30], algorithms that exploit the common bands of OLCI and MSI may increase the accuracy of surface characterization and emissivity estimation.

5. Conclusions

The urban surface cover and the urban LST are essential to map and monitor in urban climate studies. This chapter demonstrates the use of satellite Earth observation geo-spatial data to assist the study of urban climate. The methods proposed here can be easily adapted to the Sentinels, which will have high revisit rate, and thus to provide high spatial and temporal resolution LST products for urban areas. Approaches like the ones described in this chapter can become operational once adapted to Sentinels, since their long-term operation plan guarantees the future supply of satellite observations. Thus, the described methods may support planning activities related to climate change mitigation and adaptation in cities, as well as routine urban planning activities. It is therefore expected to advance the current knowledge of the impacts of the intra-urban LST variability on urban energy budget and hence on both urban heat island and energy consumption in cities.

Acknowledgements

The project leading to this application has received partial funding from the European Union's Horizon 2020 research and innovation program under grant agreement No. 637519 (URBANFLUXES) and partial funding from the project SEN4RUS (MIS T3EPA-00101) which is funded by the Operational Programme "Competitiveness, Entrepreneurship and Innovation" (NSRF 2014–2020) and co-financed by Greece and the European Union (European Regional Development Fund).

Author details

Zina Mitraka* and Nektarios Chrysoulakis

*Address all correspondence to: mitraka@iacm.forth.gr

Foundation for Research and Technology Hellas, Heraklion, Greece

References

[1] Landsberg HE. The Urban Climate. New York: Academic Press; 1981

[2] Chrysoulakis N, Marconcini M, Gastellu-Etchegorry J-P, Grimmond CSB, Feigenwinter C, Lindberg F, Del Frate F, Klostermann J, Mitraka Z, Esch T, Landier L, Gabey A, Parlow E, Olofson F. Anthropogenic heat FLUX estimation from Space. In: Proceedings of 2017 Joint Urban Remote Sensing Event, JURSE 2017; Dubai, United Arab Emirates; 6-8 March 2017. DOI: 10.1109/JURSE.2017.7924591

[3] Khamsi R. Human activity implicated in Europe's 2003 heat wave. news@nature. 2004. DOI: 10.1038/news041129-6

[4] Arnfield AJ. Two decades of urban climate research: A review of turbulence, exchanges of energy and water, and the urban heat island. International Journal of Climatology. 2003;**23**:1-26. DOI: 10.1002/joc.859

[5] Barnes KB, Morgan JM, Roberge MC, Roberge M. Impervious Surfaces and the Quality of Natural and Built Environments. Baltimore, Maryland: Towson University; 2002

[6] Santamouris M. Using cool pavements as a mitigation strategy to fight urban heat island—A review of the actual developments. Renewable and Sustainable Energy Reviews. 2013; **26**:224-240. DOI: 10.1016/j.rser.2013.05.047

[7] Hepinstall JA, Alberti M, Marzluff JM. Predicting land cover change and avian community responses in rapidly urbanizing environments. Landscape Ecology. 2008;**23**:1257-1276. DOI: 10.1007/s10980-008-9296-6

[8] Grimm NB, Faeth SH, Golubiewski NE, Redman CL, Wu J, Bai X, Briggs JM. Global change and the ecology of cities. Science. 2008;**319**:756-760. DOI: 10.1126/science.1150195

[9] Batty M. The size, scale, and shape of cities. Science. 2008;**319**:769-771. DOI: 10.1126/science.1151419

[10] Rashed T, Weeks JR, Stow D, Fugate D. Measuring temporal compositions of urban morphology through spectral mixture analysis: Toward a soft approach to change analysis in crowded cities. International Journal of Remote Sensing. 2005;**26**:699-718. DOI: 10.1080/01431160512331316874

[11] Bhatta B. Analysis of Urban Growth and Sprawl from Remote Sensing Data. Berlin, Heidelberg: Springer Science & Business Media; 2010

[12] Weng Q, editor. Global Urban Monitoring and Assessment through Earth Observation. 1st ed. Boca Raton, Florida, USA: CRC Press Taylor & Francis Group; 2014. 387 p. ISBN: 9781466564497

[13] Shannon CE. Communication in the presence of noise. Proceedings of the IRE. 1949; **37**:10-21

[14] Roberts DA, Quattrochi DA, Hulley GC, Hook SJ, Green RO. Synergies between VSWIR and TIR data for the urban environment: An evaluation of the potential for the Hyperspectral infrared imager (HyspIRI) decadal survey mission. Remote Sensing of Environment. 2012;**117**:83-101. DOI: 10.1016/j.rse.2011.07.021

[15] Powell R, Roberts D, Dennison P, Hess L. Sub-pixel mapping of urban land cover using multiple endmember spectral mixture analysis: Manaus, Brazil. Remote Sensing of Environment. 2007;**106**:253-267. DOI: 10.1016/j.rse.2006.09.005

[16] Weng Q, Hu X, Liu H. Estimating impervious surfaces using linear spectral mixture analysis with multitemporal ASTER images. International Journal of Remote Sensing. 2009;**30**:4807-4830. DOI: 10.1080/01431160802665926

[17] Drusch M, Del Bello U, Carlier S, Colin O, Fernandez V, Gascon F, Hoersch B, Isola C, Laberinti P, Martimort P, Meygret A, Spoto F, Sy O, Marchese F, Bargellini P. Sentinel-2: ESA's optical high-resolution mission for GMES operational services. Remote Sensing of Environment. 2012;**120**:25-36. DOI: 10.1016/j.rse.2011.11.026

[18] Berger M, Moreno J, Johannessen JA, Levelt PF, Hanssen RFESA. S missions in support of earth system science. Remote Sensing of Environment. 2012;**120**:84-90. DOI: 10.1016/j.rse.2011.07.023

[19] Meirich S. Mapping Guide for a European Urban Atlas. Available from: http://ec.europa.eu/regional_policy/sources/tender/pdf/2012066/annexe2.pdf [Accessed: 2017-11-29]

[20] Masek JG, Vermote EF, Saleous N, Wolfe R, Hall FG, Huemmrich F, Gao F, Kutler J, Lim TK. LEDAPS Calibration, Reflectance, Atmospheric Correction Preprocessing Code, version 2. Model product. 2013. Available from: http://daac.ornl.gov/cgi-bin/dsviewer.pl?ds_id=1146 [Accessed: 2017-11-29]

[21] Mitraka Z, Del Frate F, Carbone F. Nonlinear spectral Unmixing of Landsat imagery for urban surface cover mapping. IEEE Journal of Selected Topics in Applied Earth Observations and Remote Sensing. 2016;**9**(7):1-11. DOI: 10.1109/JSTARS.2016.2522181

[22] Small C. The Landsat ETM+ spectral mixing space. Remote Sensing of Environment. 2004; **93**:1-17. DOI: 10.1016/j.rse.2004.06.007

[23] Keshava N, Mustard JF. Spectral unmixing. IEEE Signal Processing Magazine. 2002;**19**: 44-57

[24] Heylen R, Parente M, Gader P. A review of nonlinear hyperspectral unmixing methods. IEEE Journal of Selected Topics in Applied Earth Observations and Remote Sensing. 2014;**7**:1844-1868. DOI: 10.1109/JSTARS.2014.2320576

[25] Meganem I, Déliot P, Briottet X, Deville Y, Hosseini S. Linear-quadratic mixing model for reflectances in urban environments. IEEE Transactions on Geoscience and Remote Sensing. 2014;**52**:544-558. DOI: 10.1109/TGRS.2013.2242475

[26] Mitraka Z, Chrysoulakis N, Doxani G, Del Frate F, Berger M. Urban surface temperature time series estimation at the local scale by spatial-spectral Unmixing of satellite observations. Remote Sensing. 2015;**7**:4139-4156. DOI: 10.3390/rs70404139

[27] Baldridge AM, Hook SJ, Grove CI, Rivera G. The ASTER spectral library version 2.0. Remote Sensing of Environment. 2009;**113**:711-715. DOI: 10.1016/j.rse.2008.11.007

[28] Jimenez-Munoz J-C, Sobrino JA. Split-window coefficients for land surface temperature retrieval from low-resolution thermal infrared sensors. IEEE Geoscience and Remote Sensing Letters. 2008;**5**:806-809. DOI: 10.1109/LGRS.2008.2001636

[29] Mitraka Z, Doxani G, Del Frate F, Chrysoulakis N. Uncertainty estimation of local-scale land surface temperature products over urban areas using Monte Carlo simulations. IEEE Geoscience and Remote Sensing Letters. 2016;**13**(7):1-5. DOI: 10.1109/LGRS.2016.2553367

[30] Gastellu-Etchegorry J-P, Lauret N, Yin T, Landier L, Kallel A, Malenovsky Z, Al Bitar A, Aval J, Benhmida S, Qi J, Medjdoub G, Guilleux J, Chavanon E, Cook B, Morton D, Chrysoulakis N, Mitraka Z. DART: Recent advances in remote sensing data modeling with atmosphere, polarization, and chlorophyll fluorescence. IEEE Journal of Selected Topics in Applied Earth Observations and Remote Sensing. 2017;**10**:2640-2649. DOI: 10.1109/JSTARS.2017.2685528